Perspectives for earthquake prediction in the Mediterranean and contribution of geological observations

B. C. PAPAZACHOS, G. F. KARAKAISIS, C. B. PAPAZACHOS & E. M. SCORDILIS

Geophysical Laboratory, Aristotle University, PO Box 352-1, 54124, Thessaloniki, Greece (e-mail: karakais@geo.auth.gr)

Abstract: Accelerating seismic strain caused by the generation of intermediate-magnitude preshocks in a broad (critical) region, accompanied by decelerating seismic strain caused by the generation of smaller preshocks in the seismogenic region are systematically observed before strong mainshocks. On the basis of this seismicity pattern a model has been developed that seems promising for intermediate-term earthquake prediction, called the 'Decelerating in–Accelerating out Seismic Strain Model'. Recent seismological data for the Mediterranean region are used here for backward and forward testing of this model. The selection of the broader Mediterranean region as a test area was motivated not only by the interest of time-dependent seismic hazard assessment in a high-seismicity and highly populated region but also by the fact that the Mediterranean is a natural geophysical and geological laboratory where both complex multi-plate and continuum tectonics are found in a more or less convergent zone. Within this complex geotectonic setting several geological phenomena such as subduction, collision, orogen collapse and back-arc extension take place, leading to the generation of a broad spectrum of mainshocks, reaching $M_W = 8.0$ or greater for subduction-related thrust events and a variety of corresponding seismicity levels and neotectonic activity ranging from very low (e.g. large parts of Iberian peninsula) to very high (broader Aegean area). The backward procedure shows that all six strong ($M \geq 6.8$) mainshocks that have occurred in the Mediterranean since 1980 had been preceded by preshock sequences that followed this seismicity pattern and satisfy all model constraints. Application of the model for future mainshocks has led to the identification of nine regions (in the Pyrenees, Calabria, NE Adriatic, Albania, Northern Greece, SE Aegean, NW Anatolia, western Anatolia, NE Anatolia) where current intermediate-magnitude seismicity satisfies the constraints of the model and corresponds to strong ($M \geq 6.2$) mainshocks. The magnitudes, epicentres and origin times of these probably ensuing mainshocks, as well as their corresponding uncertainties, are estimated, so that it is possible to evaluate the model potential during the next decade (2006–2015). Furthermore, it is shown that geological observations of surface fault traces can contribute to the accurate location of the foci of future strong mainshocks in the Mediterranean and to an estimation of their sizes. For this purpose, globally valid relations between fault parameters based on geological observations (surface fault length, L_S, and fault slip, u_S) and measures of mainshock size (mainshock magnitude, subsurface fault length, L, and fault slip, u) are proposed.

Recently, it has become more evident that anti-seismic measures cannot be effective without knowledge on the location, size and time of future strong earthquakes, that is, without prediction of individual strong earthquakes. At present, however, only knowledge of the spatial distribution of strong earthquakes is of practical use because their time distribution is considered as random. This is because the prediction of all three basic parameters (space, time, magnitude) with reasonable uncertainties is a very difficult scientific task.

Short-term earthquake prediction (time uncertainty of the order of days to weeks) is not feasible with the present state of knowledge (e.g. Wyss 1997). Long-term prediction (time uncertainty of the order of decades) of a future strong earthquake (mainshock) requires accurate knowledge of the physical process of generation of the previous mainshock on the same fault, but such knowledge is not feasible at present (Jaumé & Sykes 1999). It seems, however, that intermediate-term earthquake prediction (time uncertainty of the order of a few years) is possible, on the basis of precursor seismicity patterns (Evison 2001).

Accelerating generation of intermediate-magnitude preshocks in broad regions (Tocher 1959; Papadopoulos 1986; Sykes & Jaumé 1990; Knopoff *et al.* 1996; Tzanis *et al.* 2000, among many others) and decelerating generation (seismic quiescence) of preshocks in the narrower (seismogenic) region (Wyss & Habermann 1988; Bufe *et al.* 1994; Hainzl *et al.* 2000; Zöller *et al.*

From: ROBERTSON, A. H. F. & MOUNTRAKIS, D. (eds) 2006. *Tectonic Development of the Eastern Mediterranean Region*. Geological Society, London, Special Publications, **260**, 689–707.
0305-8719/06/$15.00

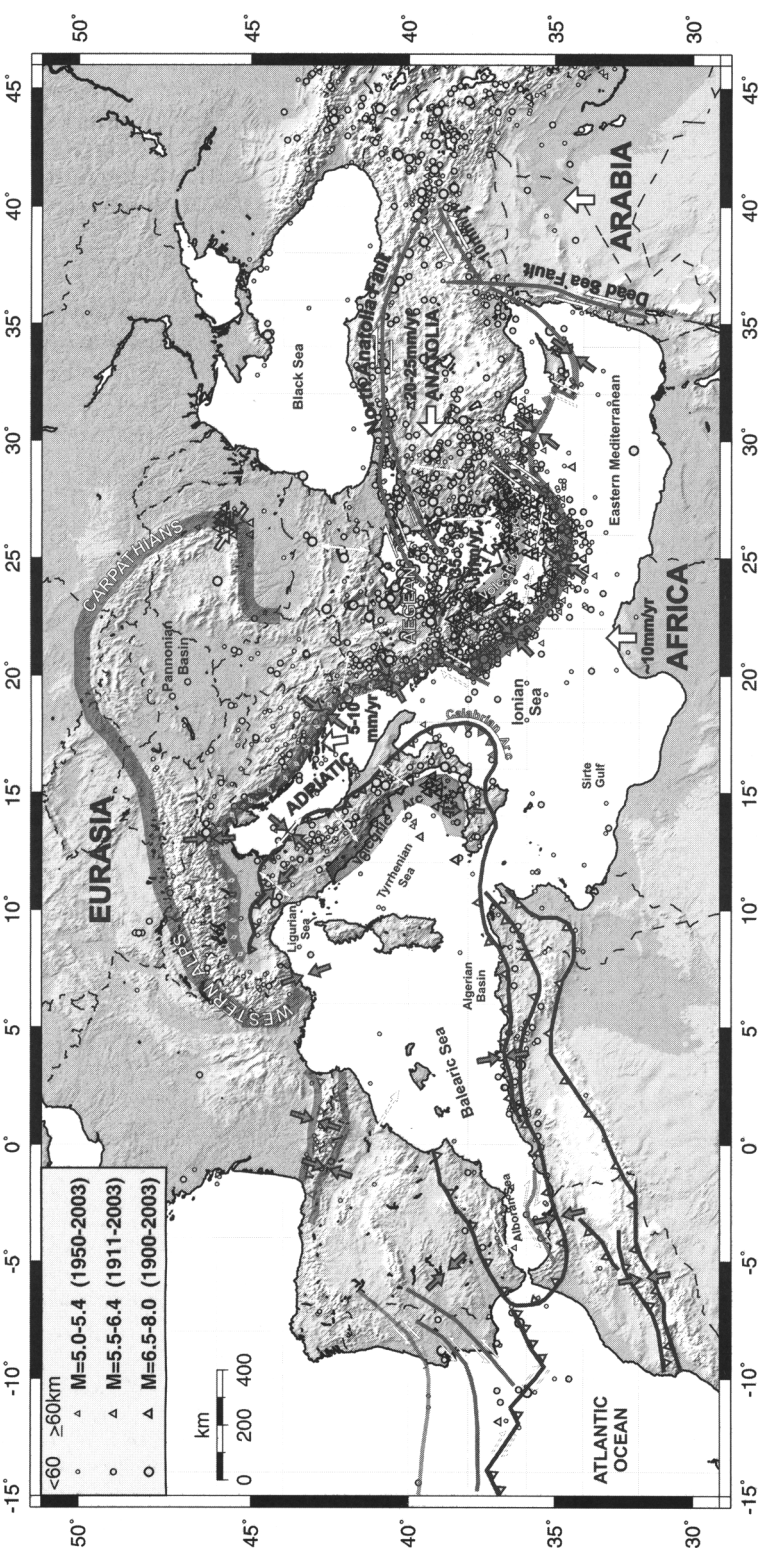

Fig. 1. Summary seismotectonic map of the Mediterranean region. Earthquakes that occurred during the instrumental period (1900–2003) are denoted by circles and triangles for shallow and intermediate depth, respectively. Major plate motions with respect to Eurasia are shown by large arrows, and local stresses and relative fault-slip are shown by double vectors. Major tectonic boundaries are modified from Jolivet & Faccenna (2000) and Papazachos & Papazachou (2003).

2002) are two of the most distinct precursory patterns. The term 'preshock' does not refer to the traditional 'foreshock' term, which corresponds to earthquakes occurring in the vicinity of the fault region a few days or months before the earthquake generation, but to the intermediate earthquake activity that occurs on a much larger scale (up to almost 10 times the fault length) within the critical region of the ensuing earthquake, which is preparing for its generation through stress alignment and long-range earthquake interactions.

The simultaneous occurrence of the two patterns (seismic excitation and seismic quiescence) in a region has been called a 'doughnut pattern' by Mogi (1969). Accelerating generation of preshocks in the broad (critical) region is considered as a critical phenomenon culminating in a mainshock (critical earthquake), and is considered as a critical point (Sornette & Sornette 1990; Sornette & Sammis 1995), whereas decrease of preshock activity in the narrower (seismogenic) region has been attributed to stress relaxation as a result of preseismic sliding (Kato *et al.* 1997; Wyss *et al.* 1981).

Recent detailed investigation of accelerating preshock sequences in broad critical regions (Papazachos & Papazachos 2000, 2001; Papazachos *et al.* 2005) and of decelerating preshock sequences in corresponding narrow seismogenic regions (Papazachos *et al.* 2004*a*,*b*) has revealed important predictive properties, observed almost simultaneously in both regions (critical and seismogenic) corresponding to the same mainshock. These properties have been formulated by analytical relations, which are the basis of a promising intermediate-term earthquake prediction model (Papazachos *et al.* 2006), which can be called the 'Decelerating in–Accelerating out Seismic Strain Model'.

This model is applied in the present study by using recent data for strong earthquakes in the Mediterranean and surrounding region (35°N–45°N, 5°W–40°E). Because the proposed model presents uncertainties that can be estimated and assessed only by studying a large number of events, tests performed on a smaller-scale area (e.g. a well-studied fault zone such as the North Anatolian Fault), where data for only a very few recent mainshocks can be used, may lead to misleading results. Furthermore, the establishment of the main model relations presented below requires a variety of seismotectonic environments where different magnitude mainshocks (large range of moment magnitude values) and different seismicity levels (large range of seismicity rate values) are found. The Mediterranean region is a natural geophysical laboratory, which allows for an efficient backward and forward testing of the model, as it includes various seismotectonic regimes (subduction, collision, back-arc extension, etc.) with a variety of strong mainshocks (up to $M_w = 8.0$ or larger) and seismicity levels ranging from very low (e.g. large parts of Iberian peninsula) to very high (wider Aegean area).

The main goal of this work is to test the above model on preshock sequences of strong mainshocks that have already occurred in the area (backward testing), as well as on probable preshock sequences of future strong mainshocks (forward testing). In addition, global relations are defined between geologically observed fault parameters (surface fault length and slip) and seismic quantities (moment magnitude, subsurface fault length and slip) (Papazachos *et al.* 2004*c*), to facilitate the contribution of geological observations to the estimation of the location and size of future mainshocks.

Study area

The Mediterranean region (Fig. 1) represents the boundary between the Eurasian and African lithospheres, and shows a complex geotectonic setting. This setting comprises several mountain belts, as well as Neogene basins that were formed by back-arc extension and/or Alpine crust collapse (e.g. Dercourt *et al.* 1986; Dewey 1988), despite the fact that no generally accepted model for the extension mechanism exists. However, the most important factor in present-day tectonics is widely accepted to be the convergence between Eurasia and Africa in a more or less north–south direction at a rate of about 10 mm a^{-1}.

Several smaller plates also contribute significantly to this tectonic setting, such as the northward motion of the Arabian plate, the westward motion of the Anatolian plate, the SW motion of the Aegean plate, the NNW motion and anticlockwise rotation of the Adriatic plate, and the expansion towards both the east and west of the western Mediterranean lithosphere (e.g. McKenzie 1970, 1972). The clearest manifestation of these plate motions is the significant seismicity level, with events exceeding $M = 8.0$ (Papazachos 1990). These events, which are the result of this complex lithospheric interaction, occur along several types of faults, such as the strike-slip faults of northern Anatolia, dip-slip faults in the continental crust system (e.g. normal faults in the Aegean or Apennine region, low-angle thrust faults in the southern coasts of the Western Mediterranean) and dip-slip faults in the lithospheric subduction regions (e.g. convex side

of the Hellenic arc). It is interesting to note that a large number of active faults (mainly of normal type) are activated as a result of strong back-arc extension (e.g. Aegean, Anatolia, Apennines), far from the compressive margins shown in Figure 1.

Figure 1 shows significant spatial variations in the seismic activity throughout the Mediterranean. Relatively low seismicity levels are found along the more or less compressive tectonic boundaries of the Western Mediterranean, such as the Pyrenees, Betics, Alboran Sea and Atlas (e.g. Andrieux *et al.* 1971; Buforn *et al.* 1988*a*,*b*; Jimenez-Munt & Negredo 2003). The Central Mediterranean shows higher activity as a result of the Inner Apennine extension, the Tyrrhenian Sea subduction and the Adriatic collision with the Dinarides (e.g. McKenzie 1972; Gasparini *et al.* 1985; Malinverno & Ryan 1986; Anderson & Jackson 1987; Faccenna *et al.* 1996, 2001; Wortmann *et al.* 2001). The fastest plate motions and corresponding seismicity levels are found in the Eastern Mediterranean, with Arabia moving northwards along the Dead Sea Fault, resulting in a transpressional regime along the East Anatolian Fault. Deformation rates and seismicity increase in the Anatolia region as a result of its westward migration, with most of its westward motion taken along the North Anatolian Fault, whereas the Aegean region exhibits the highest deformation rates and seismicity, moving rapidly towards the SW, owing to the combined effect of Anatolia westward motion and subduction rollback (McKenzie 1970, 1972; Mercier *et al.* 1976, 1989; Dewey & Şengör 1979; LePichon & Angelier 1979; Jackson & McKenzie 1988; Taymaz *et al.* 1991; Papazachos & Kiratzi 1996; Meijer & Wortel 1997; Kahle *et al.* 1998; Papazachos *et al.* 1998; McClusky *et al.* 2000).

The seismicity pattern shown in Figure 1 should not be considered as either static or representative. Significant long-term temporal seismicity variations have been identified in this area, and several large events occur on major faults with long return periods (e.g. Dead Sea Fault). Furthermore, several destructive events often occur along sections of the Mediterranean tectonic boundaries, which are considered to be of relatively low seismic hazard potential, such as the recent Morocco and Algeria events. Moreover, the exact geometry and seismicity potential of several of the tectonic boundaries shown in Figure 1, especially at sea, are still poorly understood. Therefore, it is imperative to incorporate all available and future geological information to better understand and constrain the active tectonic setting of the Mediterranean and facilitate earthquake prediction efforts.

The model

The model used in the present work has its observational basis in two precursory seismicity patterns, the 'accelerating seismic strain in a broader (critical) region' and the 'decelerating seismic strain in a narrower (seismogenic) region'. Two corresponding methods have been proposed for intermediate-term earthquake prediction. The first of these, called the 'time-to-failure method' (Bufe & Varnes 1993) is based on the accelerating generation of the Benioff strain (square root of seismic energy) released by intermediate-magnitude preshocks in the broader region. The second one, called the 'seismic quiescence method' (e.g. Wyss *et al.* 1981), is based on the decrease of the rate of generation of small preshocks in the narrower (seismogenic) region.

Both methods have been recently developed further and combined to improve their efficiency for intermediate-term earthquake prediction. Regarding the accelerating strain method, additional predictive properties, which are expressed by empirical relations (Papazachos *et al.* 2005), have been recently proposed. Also, recent developments of the seismic quiescence method consider the decelerating strain instead of the decrease of the frequency of the small preshocks as precursory pattern and have proposed predictive properties, which are also expressed by empirical relations (Papazachos *et al.* 2004*b*). The most important relative progress, however, is the identification of simultaneous occurrence of the two patterns during the preshock period (Papazachos *et al.* 2004*a*,*b*), which suggests the formation of a model with predictive properties called the 'Decelerating in–Accelerating out Seismic Strain Model'. This model is applied in the present work and its basic characteristics are briefly described.

Accelerating seismic strain

The time variation of the accelerating preshock seismic strain, S (in Joule$^{1/2}$), in the broader (critical) region is given by the relation

$$S(t) = A - B(t_c - t)^m \qquad (1)$$

where t is the time to the mainshock, t_c is the origin time of the mainshock and A, B and m are parameters that are determined by observations (Bufe & Varnes 1993). Bowman *et al.* (1998) quantified the degree of deviation of the time variation of S from linearity by proposing the minimization of a curvature parameter, C, which is defined as the ratio of the root mean square

error of the power-law fit (equation (1)) to the corresponding linear fit error.

Papazachos & Papazachos (2000, 2001) suggested additional constraints to the critical earthquake model expressed by empirical formulae, which relate parameters of the accelerating preshock sequence to the mainshock magnitude and the long-term seismicity rate in the critical region. Very recently, Papazachos and colleagues (Papazachos *et al.* 2005, 2006) used global data (from the Mediterranean, Himalayas, California and Japan) to derive the following empirical relations:

$$\log R = 0.42M - 0.30\log s_a + 1.25,\ \sigma = 0.15 \quad (2)$$

$$\log (t_c - t_{sa}) = 4.60 - 0.57\log s_a,\ \sigma = 0.10 \quad (3)$$

$$M = M_{13} + 0.60,\ \sigma = 0.20 \quad (4)$$

where R is the radius (in km) of the equivalent circle of the elliptical critical region, s_a (in Joule$^{1/2}$ per year and per 10^4 km^2) is the rate of the long-term seismic strain in the critical region, t_{sa} (in years) is the start time of the accelerating sequence, M is the mainshock magnitude and M_{13} is the mean magnitude of the three largest preshocks. The smallest preshock magnitude, M_{min}, of an accelerating preshock sequence for which the best solution is obtained is given by the relation

$$M - M_{min} = 0.54M - 1.91 \quad (5)$$

where M is the mainshock magnitude (Papazachos *et al.* 2005). Thus, for mainshock magnitudes 6, 7 and 8, the M_{min} is 4.7, 5.1 and 5.6, respectively.

The probability, P, that the calculated parameters for an examined region fit these relations is also estimated by the available data for this region. Furthermore, for each point of an investigated area a 'quality index', q_a, has been defined (Papazachos *et al.* 2002) by the formula

$$q_a = \frac{P}{mC}. \quad (6)$$

Hence, q_a increases with increasing probability, P, showing a similarity to previous preshock (critical) region behaviours, to the degree of deviation from linearity of the time variation of the strain (decrease of C), and to the degree of acceleration (decrease of m). The following cut-off values have been determined (Papazachos *et al.* 2005) for these four parameters:

$$C \le 0.60,\ P \ge 0.45,\ m \le 0.35,\ q_a \ge 3.0. \quad (7)$$

From all grid points of the examined area that fulfil these relations, the one for which the quality index, q_a, takes its largest value is considered as the geometric centre, Q, of the critical region and the corresponding solution (M, t_{sa}, M_{13}, s_a, . . .) as the best solution.

Decelerating seismic strain

Decelerating seismic strain released by intermediate-magnitude preshocks in the seismogenic region during the critical period, when accelerating seismic strain occurs in the broader region, also follows a power law (equation (1)) but with $m > 1.0$ (Papazachos *et al.*, 2006). Additional properties of the decelerating strain in the seismogenic region are expressed by the relations

$$\log a = 0.23\mathrm{M} - 0.14\log s_d + 1.40,\ \sigma = 0.10 \quad (8)$$

$$\log (t_c - t_{sd}) = 2.95 - 0.31\log s_d,\ \sigma = 0.12 \quad (9)$$

where a (in km) is the large axis of the elliptical seismogenic region (typically with ellipticity $e = 0.70$), M is the magnitude of the mainshock, t_{sd} (in years) is the start time of the preshock decelerating strain and s_d (in Joule$^{1/2}$ per year and per 10^4 km^2) is the long-term seismic Benioff-strain rate of the seismogenic region. The smallest magnitude, M_{min}, of the decelerating preshocks for which the best solution is obtained is given by the relation

$$M - M_{min} = 0.71M - 2.35,\ \sigma = 0.1 \quad (10)$$

where M is the mainshock magnitude (Papazachos *et al.* 2006). Thus, for mainshock magnitudes 6, 7 and 8, the values of M_{min} are 4.1, 4.4 and 4.7, respectively. A quality index can be also defined by the relation

$$q_d = \frac{P \cdot m}{C} \quad (11)$$

where P is the probability that decelerating preshock observations in a seismogenic region are compatible with equations (8) and (9). The following cut-off values have been determined for these parameters by the use of global data (Papazachos *et al.* 2006):

$$C \le 0.60,\ P \ge 0.45,\ 2.5 \le m \le 3.5,\ q_d \ge 3.0. \quad (12)$$

The geographical point of the narrower (seismogenic) region that fulfils equations (12) and corresponds to the largest q_d value (best solution) is considered as the geometric centre, F, of the seismogenic region.

Estimation of parameters of ensuing mainshocks

For the estimation (prediction) of the parameters of ensuing mainshocks we make use of properties of both the accelerating pattern and decelerating pattern of the seismic strain. Thus, the estimated origin time, t_c*, of the ensuing mainshock is the average of the origin time corresponding to the best solution of the accelerating seismic strain (equation (3)) and of the origin time corresponding to the best solution of the decelerating seismic strain (equation (9)). Similarly, the estimated magnitude, M*, of the ensuing mainshock is the average of the value calculated by equations (2) and (4) and equation (8).

For an estimation of the geographical coordinates of the epicentre, $E^*(\varphi, \lambda)$, of the ensuing mainshock we make use of the locations of: the geometric centre, F, of the seismogenic region; the mean epicentre, P_f, of the decelerating preshocks, which is considered as the physical centre of the seismogenic region; the geometric centre, Q, of the critical region; and the mean epicentre, P_q, of the accelerating preshocks, which is considered as the physical centre of the critical region. The two centres F and P_f are usually close, and for this reason we make use of the middle point, D, of the line segment F-P_f. For the same reason, we make use of the middle point, A, of Q-P_q. From a large sample of previous mainshocks (Papazachos *et al.* 2006) it has been shown that the mean distance between D and the mainshock epicentre is $DE = 100$ km with a standard deviation of 40 km, and the distance between A and E is AE = 180 km with a standard deviation of 80 km. Then, the mainshock epicentre, E, is defined by the circle (D, 100 km) with centre D and radius 100 km and by the circle (A, 180 km). In the cases when the two circles intersect at two close points or these circles do not intersect there is a unique solution. In these cases, the estimated epicentre is considered to be the intersection of circle (D, 100 km) with the line DA that is closer to the circle (A, 180 km). The mainshock epicentre, E, lies between D and A at a mean distance DE = 0.4 DA.

From comparison of the estimated parameters (t_c*, M*, E*) using this approach of previous mainshocks with the known parameters (t_c, M, E) of these mainshocks, it can be concluded (Papazachos *et al.* 2006) that the two standard deviation model uncertainties for the estimated parameters are ± 2.5 years for the origin time of the mainshock, ± 0.4 for the magnitude and 80 ± 70 km for its epicentre. These uncertainties can be also adopted for the nine probably ensuing mainshocks considered in the present work, as an indication of the accuracy of the proposed predictions.

Application of the model for earthquakes of the Mediterranean

As it is not possible to test the validity of an earthquake prediction model by producing data at will (for instance, by laboratory experiments), retrospective predictions of previous earthquakes (postdictions) or predictions of future earthquakes are usually used instead. Both these procedures are examined in the present work. For this reason, three data samples are necessary for the study area: (1) a sample that includes the examined mainshocks; (2) a sample containing the preshocks of each mainshock; (3) all shocks that are used to define the long-term mean strain rate release both in each critical region, s_a, and in the seismogenic region that engulfs each fault, s_d.

For the purposes of the present work, data for the broader Mediterranean region have been taken from a recently compiled catalogue for this region (Papazachos *et al.* 2005). The standard catalogue uncertainties involved are typically less than 30 km for the epicentre and 0.3 for the moment magnitude. It should be noted that the data necessary to compute the long-term mean strain release ($M \geq 5.2$) are complete since 1911 for the Mediterranean region (Western Mediterranean, Aegean, Anatolia). Furthermore, all magnitudes reported in the catalogue are either originally reported moment magnitudes or equivalent to moment magnitudes; that is, magnitudes that have been transformed to moment magnitudes from any other available scale (usually M_s or m_b published by the International Seismological Center, ISC, and/or National Earthquake Information Center, NEIC) by using appropriate formulae (Scordilis 2006); this ensures the proper computation of Benioff strain from the earthquake catalogue.

Backward testing

Such testing, to be reliable, must be applied to a complete sample of mainshocks. All shallow mainshocks with $M \geq 6.8$ that occurred in the Mediterranean and surrounding area (35°N–45°N, 5°W–40°E) since 1980 have been considered as such a sample. The minimum magnitude, 6.8, and the minimum time, 1980, have been defined to have high accuracy and completeness of the available data used for the study area.

In the first line of each of the six cases presented in Table 1, the date, the geographical coordinates of the epicentre and the magnitude of these six mainshocks are given. In the second line,

Table 1. *Parameters of the critical regions (second line in each case) where accelerating preshock seismic deformation has been observed and of the seismogenic regions (third line in each case) where decelerating preshock seismic deformation has been observed before the generation of the six large ($M \geq 6.8$) mainshocks (first line in each case) that occurred in the Mediterranean region between 1980 and 2003*

Event	Date	φ, λ	M	a	z	e	C	m	q	M_{min}	n	t_s	Log s_r
1	10.10.1980	36.2, 01.4	7.1										
	Algeria	36.4, 05.7	7.3	1314	100	0.95	0.51	0.3	3.4	5.5	29	1911	4.5
		36.2, 01.6		138	100	0.70	0.58	2.8	4.5	4.4	60	1944	5.2
2	23.11.1980	40.8, 15.3	6.9										
	Italy	43.5, 14.3	6.9	443	140	0.70	0.45	0.3	4.9	5.1	81	1951	5.3
		40.6, 15.1		123	130	0.70	0.56	2.8	2.5	4.3	49	1958	5.7
3	19.12.1981	39.0, 25.3	7.2										
	N Aegean	40.0, 24.3	7.2	362	40	0.70	0.47	0.3	4.6	5.2	44	1969	5.9
		39.6, 24.5		89	40	0.70	0.42	3.4	4.4	4.5	83	1964	6.0
4	17.1.1983	38.1, 20.2	7.0										
	W Greece	38.6, 17.8	7.1	391	0	0.70	0.32	0.3	6.4	5.1	61	1963	5.6
		38.2, 20.1		36	50	0.70	0.40	3.0	3.3	4.5	58	1970	6.2
5	9.10.1996	34.5, 32.1	6.8										
	Cyprus	35.5, 30.6	6.7	324	150	0.70	0.49	0.3	3.3	5.0	40	1981	5.6
		34.3, 32.3		71	40	0.70	0.42	2.5	2.5	4.2	16	1963	5.3
6	17.8.1999	40.8, 30.0	7.4										
	Anatolia	38.8, 28.4	7.6	1089	90	0.90	0.30	0.3	5.5	5.1	181	1988	5.8
		40.8, 29.8		129	90	0.70	0.32	3.2	8.7	4.6	17	1980	5.8

the parameters for the broader (critical) region are listed: φ, λ are the geographical coordinates of the centre, Q, of the critical region, M is the predicted magnitude, a (in km) is the length of the large axis of the elliptical critical region, z is the azimuth of this axis, e is the ellipticity of the region, C is the curvature parameter, m is the parameter from equation (1), q is the quality index, M_{min} is the minimum preshock magnitude, n is the number of preshocks, t_s is the start year of the preshock sequence and s_r (in Joule$^{1/2}$ per years and per 10^4 km^2) is the long-term strain rate. In the third line of each of the six cases presented in Table 1 the corresponding parameters for the narrow (seismogenic) elliptical regions are presented, such as the geographical coordinates of the geometric centre of this region, and the length, a, of the large axis of the seismogenic region.

Figure 2 shows the broader (critical) and the narrower (seismogenic) elliptical regions for the six strong mainshocks in the Mediterranean. In the same figure the time variation of the cumulative strain, $S(t)$, in the critical regions (accelerating strain, upper part of Fig. 2) and in the seismogenic regions (decelerating strain, lower part of Fig. 2) are also shown. Open circles and dots in this figure show epicentres of accelerating and decelerating preshocks, respectively. Numbers in Figure 2 correspond to code numbers of mainshocks in Table 1, and stars denote the epicentres of the six mainshocks.

The procedure followed in the present work considers the generation (in the broader critical region) of accelerating strain that satisfies equations (7) and the generation (in the narrower seismogenic region) of decelerating strain that satisfies equations (12). Preshock activity associated with all six strong ($M \geq 6.8$) mainshocks that occurred in the Mediterranean region during the period 1980–2003 fulfils constraints imposed by the model, as parameters C, m, P and q calculated for each preshock sequence (see Table 1) satisfy these relations. Therefore, the backward test can be considered as successful.

Forward testing

For a forward testing of the model of Decelerating in–Accelerating out Seismic Strain, all of the Mediterranean and surrounding region (35°N–45°N, 5°W–40°E) has been separated into a grid of points (0.2° × 0.2°), and each point has been considered as the centre of an elliptical critical region corresponding to mainshocks with $M \geq 6.2$. Nine groups of points that fulfil equations (7) have been identified (Pyrenees, Calabria, NE Adriatic, Albania, Northern Greece, SE Aegean, NW Anatolia, Western Anatolia, NE Anatolia). The point for each group, which corresponds to the best solution (largest q_a value) is considered as the geometric centre, Q, of the corresponding elliptical critical region. Information

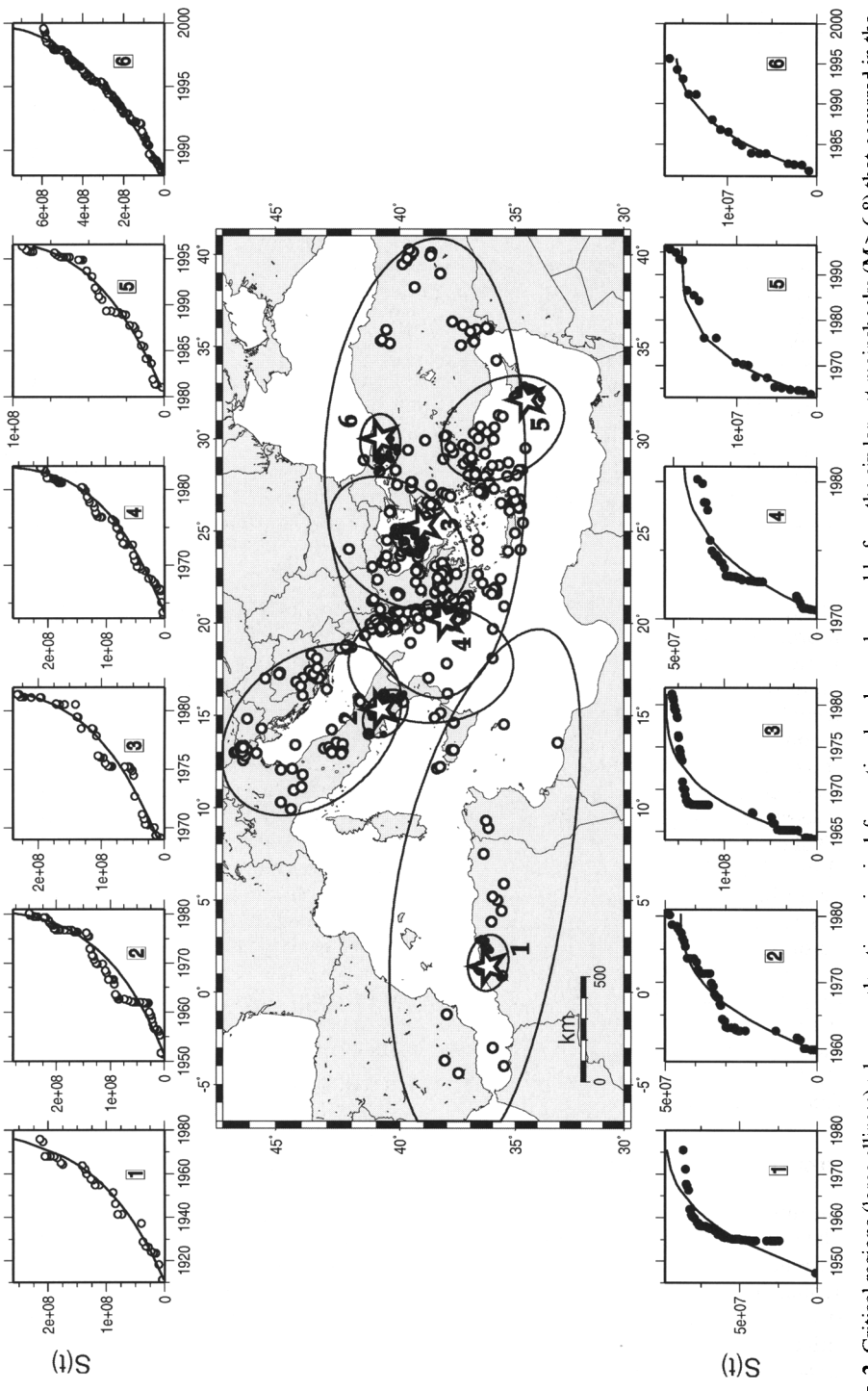

Fig. 2. Critical regions (large ellipses) where accelerating seismic deformation has been observed before the six largest mainshocks ($M \geq 6.8$) that occurred in the Mediterranean area since 1980 and corresponding seismogenic regions (small ellipses) where decelerating deformation has been observed before these mainshocks. Small open circles and dots show epicentres of accelerating and decelerating preshocks, respectively. The corresponding time variations of the accelerating and decelerating Benioff strain, *S*, are shown in the upper and lower part of the figure, respectively. The numbers correspond to the code numbers of Table 1, where information on the relevant parameters is given.

Table 2. *Parameters of the critical regions (first line in each case) where accelerating seismic deformation currently occurs and parameters of the seismogenic regions (second line in each case) where decelerating seismic deformation currently occurs in the Mediterranean region*

Event	t_c	φ, λ	M	a	z	e	C	m	q	M_{min}	n	t_s	Log s_r
1	2009.0	43.2, 09.2	6.4	397	90	0.90	0.42	0.3	6.4	4.8	59	1964	5.17
	2007.2	42.5, 01.5	6.5	248	80	0.70	0.21	3.0	13.5	4.2	38	1963	5.27
2	2008.3	38.2, 17.6	6.8	292	100	0.60	0.50	0.3	6.4	4.9	38	1984	5.64
	2009.6	38.6, 15.6	6.6	174	60	0.70	0.34	3.0	7.5	4.3	37	1991	5.42
3	2008.5	43.5, 14.0	6.5	297	20	0.70	0.42	0.3	7.4	4.9	52	1972	5.33
	2008.7	44.6, 16.1	6.5	170	130	0.70	0.28	3.0	10.4	4.3	44	1988	5.27
4	2009.0	44.1, 22.4	6.6	349	10	0.60	0.37	0.3	7.0	4.9	42	1944	4.89
	2008.6	40.7, 20.5	6.6	155	20	0.70	0.36	3.0	7.5	4.3	141	1994	5.76
5	2009.2	41.0, 25.5	6.3	209	50	0.60	0.41	0.3	5.9	4.7	35	1987	5.71
	2007.1	40.9, 23.4	6.7	154	130	0.70	0.38	3.0	6.7	4.3	48	1993	5.81
6	2009.0	36.3, 26.0	7.0	533	30	0.70	0.32	0.3	7.0	5.0	141	1988	5.75
	2010.2	37.8, 26.8	6.7	160	10	0.70	0.31	3.0	6.1	4.2	497	1996	5.80
7	2009.0	42.6, 26.8	6.3	250	–	0.00	0.33	0.3	9.5	4.7	35	1957	5.06
	2008.0	41.1, 27.8	6.3	133	50	0.70	0.45	3.0	5.6	4.2	45	1993	5.72
8	2008.4	39.4, 29.6	6.2	183	60	0.70	0.46	0.3	5.8	4.7	86	1986	5.70
	2006.6	38.8, 29.5	6.2	118	100	0.70	0.30	3.0	5.7	4.1	55	1992	5.76
9	2009.0	39.6, 38.3	7.1	525	80	0.70	0.29	0.3	10.2	5.1	82	1977	5.43
	2008.6	40.8, 38.7	6.9	201	130	0.70	0.46	3.0	6.2	4.2	43	1990	5.42

on the values of the parameters of the best solution for the nine broad critical regions are listed in the first line for each of the nine cases in Table 2.

Each grid point defined in the previous step has been considered as the centre of the elliptical seismogenic region, and the point for which equations (12) hold and the quality index, q_d, has the largest value is considered as the geometric centre, F, of the seismogenic region. The nine ellipses in Figure 3 show the probable seismogenic regions defined by this method for the nine probably ensuing mainshocks. The time variation of the cumulative strain, S, in the corresponding nine assumed seismogenic regions is also shown. In the second line of each of the nine cases listed in Table 2, the parameters of the decelerating seismic strain are given.

The estimated (predicted) by this method parameters (t_c*, E*, M*) of the nine probably ensuing mainshocks are listed in Table 3.

Contribution from geological observations

Prediction of an individual earthquake requires knowledge of the source location, its size and its origin time before its generation. Because earthquakes are generated by slip on seismic faults and generation of strong shallow earthquakes on land is associated with observable surface fault traces, geological observations can contribute to the estimation of the location of the foci of strong earthquakes. The surface fault length, L_s, and surface fault slip, u_s, can be also estimated by geological observations and as these fault parameters are related to the magnitude of the maximum earthquake on the fault, the expected mainshock magnitude, M, can also be assessed by geological observations. Active faults where no strong earthquakes have occurred during the instrumental period, and that have considerable probability of generating such earthquakes in the near future, can be reliably located by geological observations, whereas only faults that have been recently activated can be identified by seismological methods (e.g. spatial distribution of aftershocks).

However, geological observations must be very carefully handled if they are to be reliably used for the estimation of seismic parameters (e.g. earthquake magnitude), because two important issues must be considered, as follows.

(1) It is well known (e.g. Wells & Coppersmith 1994; Ambraseys & Jackson 1998) that the surface fault length, L_s, and surface fault slip, u_s, are usually only a part of the real (subsurface) fault length, L, and fault slip, u. Observed values of L_s and u_s vary significantly for the same mainshock magnitude. This holds particularly for the estimation of the mean surface slip for which even secondary ground effects have sometimes been considered for the calculation of the mean fault slip. Relative errors can be considerably reduced by excluding outliers through valid statistical procedures, which take into

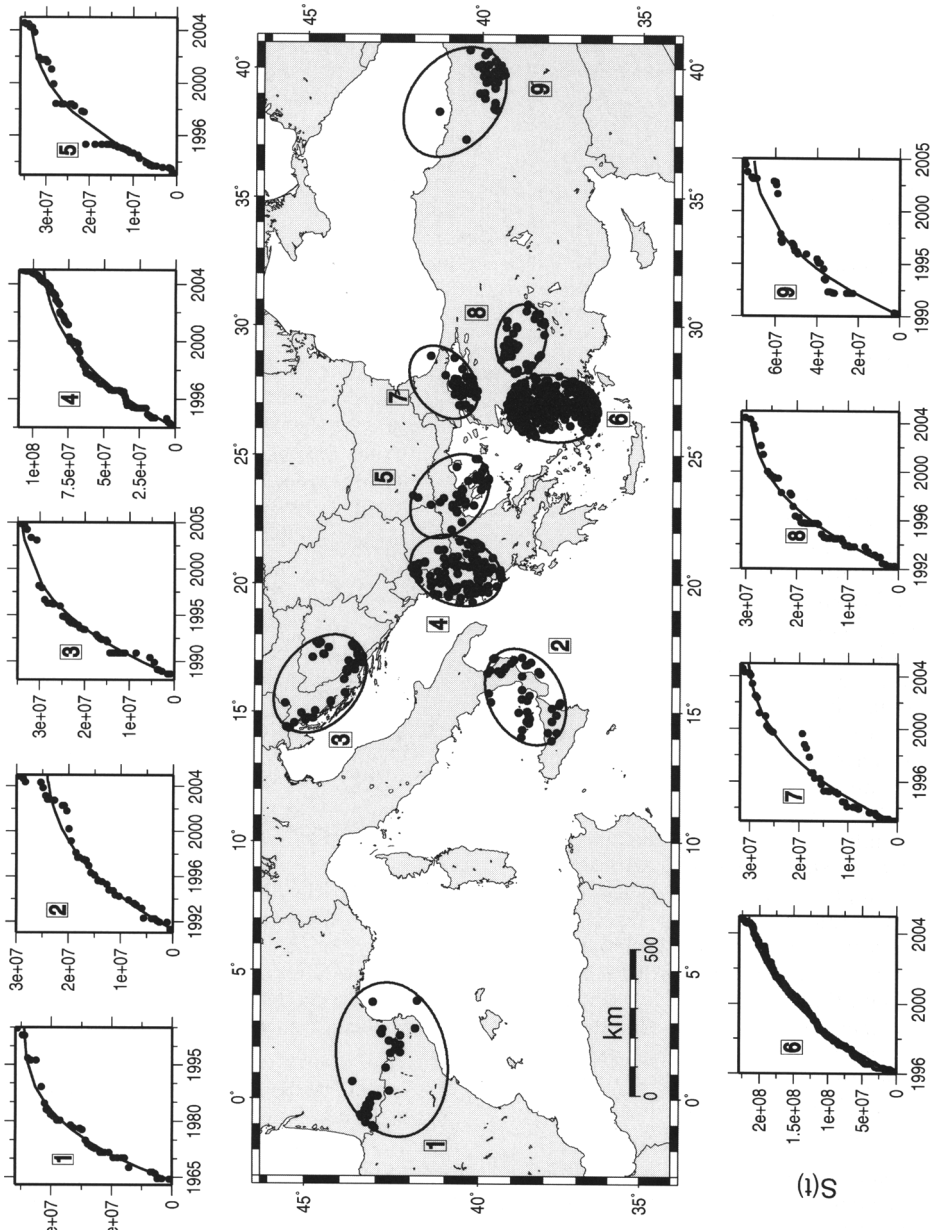

Fig. 3. Seismogenic regions (ellipses) where decelerating seismic deformation currently occurs in the eastern Mediterranean. Epicentres of decelerating shocks are shown by small dots. Corresponding time variations of decelerating Benioff strain are shown in the upper and lower part of the figure. The numbers correspond to the code numbers of Table 2, where information on the relevant parameters is given.

Table 3. *The estimated origin time, t_c*, epicentre coordinates, E*(φ, λ), and magnitude, M*, for each of the nine probably ensuing mainshocks in the Mediterranean and surrounding regions*

Event	Area	t_c*	E*(φ, λ)	M*
1	Pyrenees	2008.1	42.8°N, 02.1°E	6.4
2	Calabria	2008.9	38.5°N, 16.8°E	6.7
3	NE Adriatic	2008.6	44.1°N, 15.5°E	6.5
4	Albania	2008.8	40.1°N, 20.5°E	6.6
5	N Greece	2008.1	40.3°N, 24.7°E	6.7
6	SE Aegean	2009.6	37.2°N, 26.7°E	6.6
7	NW Anatolia	2008.5	40.9°N, 27.7°E	6.3
8	W Anatolia	2007.5	38.8°N, 29.5°E	6.2
9	NE Anatolia	2008.8	40.3°N, 39.2°E	7.0

Model uncertainties are: ±2.5 years for the origin time, ≤150 km for the epicentre and ±0.4 for the magnitude of each expected mainshock.

consideration relations between geological observations and independently estimated fault and seismic parameters. In the present work, geological observations (L_s, u_s) are compared with both real fault parameters (L, u) and moment magnitude, M.

(2) Relations between fault parameters and earthquake size depend strongly on the type of faulting, as well as on the seismotectonic environment in which these faults are found. For instance, thrust faults from continental regions have different properties from those in subduction regions, where shallow earthquakes occur along low-angle megathrust faults. Recently, Papazachos *et al.* (2004*c*) have shown that different scaling relations apply for strike-slip faults, dip-slip faults in continental regions and dip-slip faults in regions of lithospheric subduction. Furthermore, dip-slip faults in continental regions have the same scaling-law behaviour whether they are normal or thrust. It is therefore interesting to investigate the corresponding behaviour of the fault length and surface displacement based on geological observations.

In the present work, information collected from field geological observations for the fault length and surface displacement (L_s, u_s) is correlated with corresponding fault parameters (L, u), as these are defined from independent information (aftershock activity, fault parameters derived from waveform inversion), which can evaluate the 'true' subsurface fault parameters. Their dependence on the moment magnitude, M, is also examined. Following Papazachos *et al* (2004*c*), we examine separately the corresponding relations for dip-slip faults (normal or thrust) in continental regions and for strike-slip faults. Unfortunately, no direct geological observations (L_s, u_s) are available for faults in lithospheric subduction regions.

Geological data for L_s and u_s have been reported by many researchers world-wide (e.g. Wells & Coppersmith 1994; Stock & Smith 2000; Papazachos & Papazachou 2003; Pavlides & Caputo 2004). The values of surface fault length, L_s, and surface fault displacement, u_s, reported in these papers and for which reliable moment magnitudes were available are presented in Table 4 and have been used here. It should be noted that one could potentially examine the scaling-law behaviour of reverse and normal dip-slip faults separately. However, because of the limited amount of geological field information available for reverse faults in continental areas, we adopted the approach of Papazachos *et al.* (2004*c*), who showed that these two faulting types have almost indistinguishable scaling relations for their total length and displacement as these have been derived from independent information.

Relation of fault length to magnitude

Figure 4a shows a plot of the surface fault length (dots) as a function of moment magnitude for strike-slip faults. The continuous line corresponds to the relation between the real (subsurface) fault length, L, and moment magnitude (Papazachos *et al.* 2004*c*):

$$\log L = 0.59\mathrm{M} - 2.30 \qquad (13)$$

which also appears to fit the data of surface fault lengths for M ~ ≥7.5. The dashed line is a fit to the data for M ≤ 7.5 using the slope of equation (13), corresponding to the relation

$$\log L_s = 0.59\mathrm{M} - 2.50,\ 5.8 \le \mathrm{M} \le 7.5,\quad n = 28,\ \sigma = 0.18 \qquad (14)$$

where n is the number of observations and σ is the standard deviation.

Figure 4b shows the surface fault length against moment magnitude for dip-slip faults in continental regions. The continuous line is the relation between the length, L, of the real (subsurface) dip-slip fault and magnitude (Papazachos *et al.* 2004*c*):

$$\log L = 0.50\mathrm{M} - 1.86 \qquad (15)$$

which also appears to fit the data of surface fault lengths for M ~ ≥7.3, whereas the dashed line is

Table 4. *Date, epicentre coordinates, moment magnitude, M, fault parameters and region of the 48 dip-slip earthquakes and 47 strike-slip earthquakes for which data are used in the present study*

Event	Year	Date–Time	Lat.	Long.	M	L_S	u_S	KF	Region	Reference
1	1904	0404102600.0	41.90	23.00	7.3	25	10	N	Bulgaria	7
2	1906	0418131200.0	38.00	−123.00	7.9	430	330	S	California	1
3	1920	1216120543.0	35.79	105.74	8.0	220	720	S	China	1
4	1928	0414093000.0	42.15	25.28	6.8	38	–	N	Bulgaria	7
5	1928	0418192248.0	42.10	25.00	7.0	50	–	N	Bulgaria	7
6	1929	0501153722.0	37.70	57.80	7.3	70	210	T	Iran	8
7	1931	0810211840.0	47.00	90.00	7.9	180	740	S	China	1
8	1932	0926192042.0	40.45	23.86	7.0	20	30	N	Greece	7
9	1939	1226235721.0	39.50	38.50	7.8	360	–	S	Turkey	1
10	1941	0216163859.0	33.40	58.90	6.1	12	–	S	Iran	8
11	1941	0301035247.0	39.67	22.54	6.3	7	–	N	Greece	7
12	1943	1126222036.0	41.00	34.00	7.6	280	–	S	Turkey	1
13	1944	0201032236.0	41.50	32.50	7.6	180	180	S	Turkey	1
14	1944	0625041619.0	39.15	29.46	6.1	18	10	N	Turkey	7
15	1947	0923122810.0	33.70	58.70	6.8	20	128	S	Iran	8
16	1949	0822040111.0	53.75	−133.25	8.1	440	–	S	Queen Charlotte Is.	4
17	1951	1118093543.0	31.00	90.50	7.7	140	800	S	China	1,3
18	1952	0721115211.0	35.10	−118.90	7.4	57	60	R	California	1,3
19	1953	0318190613.0	40.00	27.30	7.4	–	280	S	Turkey	6
20	1954	0430130236.0	39.28	22.29	7.0	–	100	N	Greece	6
21	1954	0706111318.0	39.50	−118.50	6.2	18	25	N	Nevada	1,3
22	1954	0824055130.0	39.50	−118.30	6.9	34	45	N	Nevada	1
23	1954	1216110712.0	39.20	−118.00	7.2	57	280	S	Nevada	1
24	1954	1216111133.0	39.20	−118.00	6.9	45	210	S	Nevada	1
25	1955	0716070710.0	37.55	27.15	6.9	35	–	N	Turkey	7
26	1956	0209143239.0	31.90	−115.80	6.6	22	50	S	Mexico	1
27	1957	0526063334.0	40.67	30.86	7.0	40	55	S	Turkey	1
28	1957	1204033748.0	45.21	99.24	8.1	236	650	S	Mongolia	1,9
29	1958	0710061556.0	58.36	−136.34	7.8	95	–	S	Alaska	1,3
30	1959	0818063715.0	44.67	−110.83	7.3	27	214	N	Montana	1
31	1962	0901150058.0	25.60	65.22	7.4	99	–	R	Iran	1
32	1964	1006143123.0	40.30	28.23	6.9	40	–	S	Turkey	6
33	1966	0628042616.3	35.88	−120.42	6.4	38	–	R	California	1
34	1966	0628042616.3	35.88	−120.42	6.3	39	–	S	California	1
35	1966	0819122210.5	39.17	41.56	6.9	30	–	N	Turkey	1
36	1966	0901142257.0	37.39	22.14	6.0	2	–	N	Greece	7
37	1966	0912164101.5	39.40	−120.16	6.0	10	–	S	California	1,3
38	1967	0105001440.1	48.22	102.90	7.0	34	–	S	Mongolia	1,3
39	1967	0722165658.0	40.67	30.69	7.4	54	163	S	Turkey	1,3
40	1967	1130072350.0	41.39	20.46	6.3	16	–	N	Albania	7
41	1968	0409022900.2	33.22	−116.19	6.6	31	18	S	California	1
42	1968	0831104741.3	34.15	59.01	7.2	80	230	S	Iran	1
43	1968	1014025851.8	−31.54	117.00	6.6	36	90	R	Australia	1
44	1969	0328014829.5	38.55	28.46	6.6	32	40	N	Turkey	1,6
45	1970	0104170039.4	24.12	102.49	7.3	48	210	S	China	1,3
46	1970	0328210223.5	39.21	29.51	7.1	45	180	N	Turkey	3,6
47	1971	0209140040.6	34.40	−118.43	6.6	16	150	S	California	1
48	1971	0512062515.0	37.70	30.00	6.2	–	14	N	Turkey	7
49	1971	0522164359.3	38.85	40.52	6.6	38	–	S	Turkey	1
50	1973	0206103707.2	31.33	100.49	7.5	89	130	S	China	1
51	1973	0714045120.0	35.16	86.40	7.0	27	–	N	China	3
52	1975	0906092012.0	38.51	40.77	6.6	26	50	N	Turkey	1
53	1976	0204090143.9	15.28	−89.19	7.6	235	260	S	Guatemala	1
54	1976	1124122215.6	39.05	44.04	7.2	55	205	S	Turkey	1,3
55	1977	1219233433.3	30.93	56.48	5.9	12	12	S	Iran	1
56	1978	0523233411.4	40.73	23.25	5.8	–	10	N	Greece	6
57	1978	0620200321.5	40.78	23.24	6.5	–	30	N	Greece	6
58	1978	0916153556.7	33.37	57.44	7.4	85	150	R	Iran	1

Table 4. *Continued*

Event	Year	Date–Time	Lat.	Long.	M	L_S	u_S	KF	Region	Reference
59	1979	0602094758.7	−30.73	117.21	6.1	15	50	R	Australia	1
60	1979	0806170522.8	37.13	−121.51	5.8	14	–	S	California	1,2
61	1979	1015231657.9	32.86	−115.46	6.5	31	18	S	California	1,2,4
62	1979	1114022118.2	34.03	59.81	6.6	17	–	S	Iran	1,3
63	1979	1127171033.0	34.08	59.79	7.2	65	120	R	Iran	1,3
64	1980	0124190009.2	37.77	−121.70	5.8	6	–	S	California	1
65	1980	0709021157.4	39.29	22.91	6.5	8	21	N	Greece	8
66	1980	1010122522.1	36.16	1.40	7.1	31	154	R	Algeria	1
67	1980	1123183452.2	40.86	15.33	6.9	38	64	N	Italy	1
68	1981	0123211352.0	30.89	101.15	6.6	44	–	S	China	1
69	1981	0224205337.0	38.23	22.97	6.7	–	60	N	Greece	6
70	1981	0225023553.5	38.17	23.12	6.4	19	–	N	Greece	1
71	1981	0304215807.2	38.24	23.26	6.3	–	60	N	Greece	6
72	1981	0611072425.1	29.90	57.72	6.6	15	–	R	Iran	1
73	1981	0728172223.0	29.99	57.77	7.1	65	–	R	Iran	1
74	1982	1213091250.9	14.67	44.23	6.3	15	–	N	N Yemen	1
75	1983	1028140607.4	44.10	−113.81	6.9	34	80	N	Idaho	1
76	1983	1030041228.1	40.35	42.18	6.7	12	–	S	Turkey	1
77	1983	1222041129.3	11.85	−13.51	6.2	9	45	S	W Africa	1
78	1985	1027193457.2	36.43	6.78	6.0	–	10	S	Algeria	1
79	1986	0330085352.0	−26.30	132.77	5.8	13	–	S	Australia	1
80	1986	0913172434.3	37.08	22.15	6.0	15	12	N	Greece	6
81	1987	0302014234.7	−37.93	176.78	6.5	18	–	N	New Zealand	1,5
82	1987	1124015416.7	33.23	−115.65	6.2	10	–	S	California	1,4
83	1987	1124131556.6	33.12	−116.02	6.6	27	54	S	California	1,5
84	1988	0122003558.1	−19.82	133.86	6.3	10	63	R	Australia	1
85	1988	0122035725.6	−19.78	133.92	6.4	7	60	R	Australia	1
86	1988	0122120458.0	−19.80	133.95	6.6	16	93	R	Australia	1
87	1988	1106130319.9	22.80	99.59	7.1	35	70	S	China	1
88	1988	1106131542.0	23.20	99.46	6.8	16	60	S	China	1
89	1988	1207074124.3	40.96	44.16	6.8	25	–	R	Armenia	1
90	1989	1225142432.8	60.07	−73.48	6.0	10	–	R	Canada	1
91	1990	0716072634.7	15.70	121.22	7.7	120	–	S	Philippines	1
92	1992	0628115735.9	34.25	−116.48	7.3	71	295	S	California	1,2
93	1995	0615001549.0	38.27	22.15	6.4	7	1	N	Greece	7
94	1995	1001155712.6	38.06	30.15	6.2	11	12	N	Turkey	7
95	1999	0817000138.6	40.76	29.96	7.5	100	300	S	Turkey	6

References: 1, Wells & Coppersmith (1994); 2, Pegler & Das (1996); 3, Stock & Smith (2000); 4, Fujii & Matsuura (2000); 5, Henry & Das (2001); 6, Papazachos & Papazachou (2003); 7, Pavlides & Caputo (2004); 8, Ambraseys & Jackson (1998); 9, present study.
KF is the kind of faulting (N for normal fault, R for reverse, S for strike-slip), L_S is the length (in km) of the surface trace of the fault, and u_s is the mean slip (in cm) on the surface fault trace.

a fit to the data (dots) for $M \leq 7.3$, corresponding to

$$\log L_s = 0.59M - 2.01,\ 6.0 \leq M \leq 7.3,\ n = 37,\ \sigma = 0.22. \quad (16)$$

Relation of fault slip to magnitude

Figure 5a shows the distribution of surface fault slip v. magnitude for strike-slip faults. The continuous line shows such variation for real (subsurface) fault slip, u, (Papazachos *et al.* 2004*c*):

$$\log u = 0.68M - 2.59 \quad (17)$$

whereas the dashed line is a fit (using the slope of 0.68) to the observed surface slips, u_s, for $M \leq 7.6$, corresponding to

$$\log u_s = 0.68M - 2.76,\ 5.8 \leq M \leq 7.6,\ n = 23,\ \sigma = 0.25. \quad (18)$$

Figure 5b shows the corresponding variation of the surface fault slip with the magnitude for dip-slip faults in continental regions. The continuous line is the relation between the

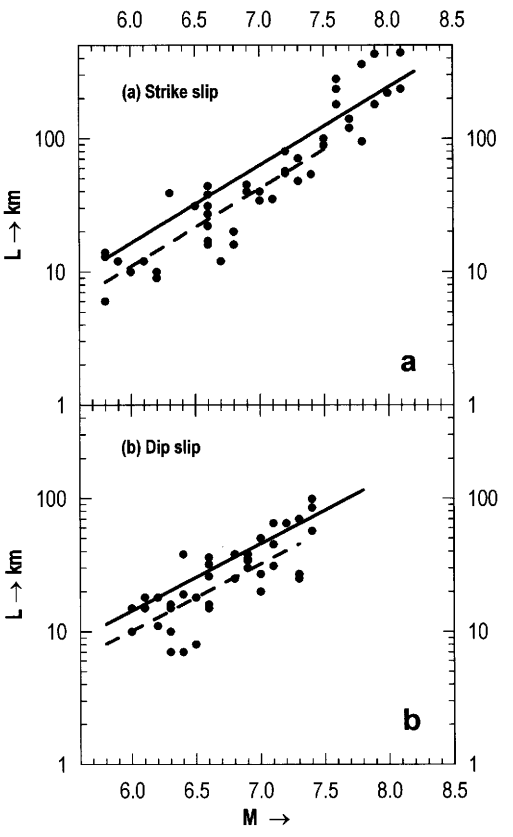

Fig. 4. Variation of observed length (in km) of surface fault traces with the moment magnitude (dots) for strike-slip faults (**a**) and dip-slip faults (**b**). Continuous lines show the variation with magnitude of the real (subsurface) fault length, L; dashed lines show the corresponding variation of the surface fault length, L_s, for the low-magnitude part of the data (see text for explanation).

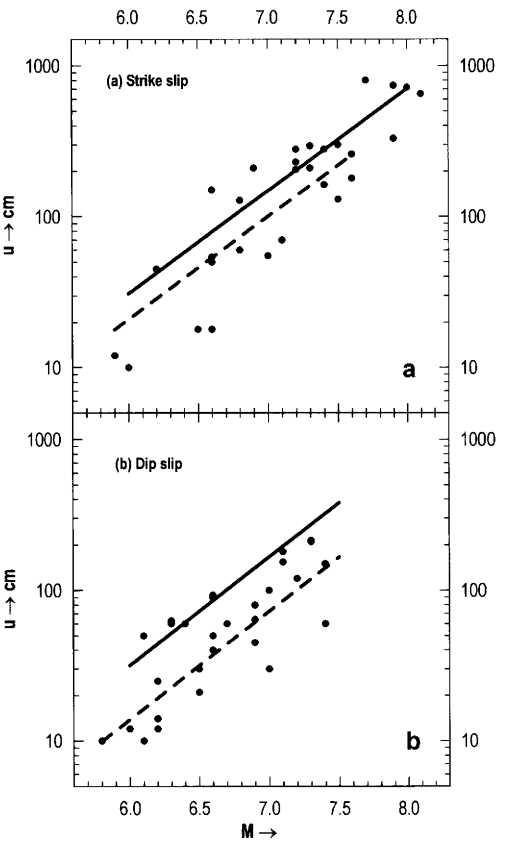

Fig. 5. Variation of observed surface fault slip (in cm) with the moment magnitude (dots) for strike-slip faults (**a**) and dip-slip faults (**b**). Continuous lines show the variation with magnitude of the real (subsurface) fault slip, u; dashed lines show the corresponding variation of the surface fault slip, u_s, for the low-magnitude part of the data (see text for explanation).

real (subsurface) fault slip and the magnitude (Papazachos *et al.* 2004*c*), which is

$$\log u = 0.72\mathrm{M} - 2.82. \qquad (19)$$

The relation fitting the surface fault slip data is

$$\log u_s = 0.72\mathrm{M} - 3.18,\ 5.8 \le \mathrm{M} \le 7.4,\quad n = 29,\ \sigma = 0.42. \qquad (20)$$

All previous results suggest that the observed fault length and slip both in strike-slip and dip-slip faults in continental areas bear a rather complex relation to the true fault length and width. This is mainly due to the fact that for smaller earthquakes the probability for a surface fault trace becomes increasingly smaller (e.g. Wells & Coppersmith 1994) and when the rupture does reach the surface, the observed fault trace length and slip is a fraction of the true length and slip, which also depends on the mainshock magnitude. To further examine this dependence, in Figure 6a and b the ratio of the observed fault length and slip to the length calculated by equations (13) and (15) for length, and calculated by equations (17) and (19) for slip are presented for both types of faults examined here (strike-slip and dip-slip) as a function of magnitude. As the logarithm of these quantities is typically considered to be related to magnitude, a log-scale is used in the plots. Despite the data scatter, there appears to be a general agreement

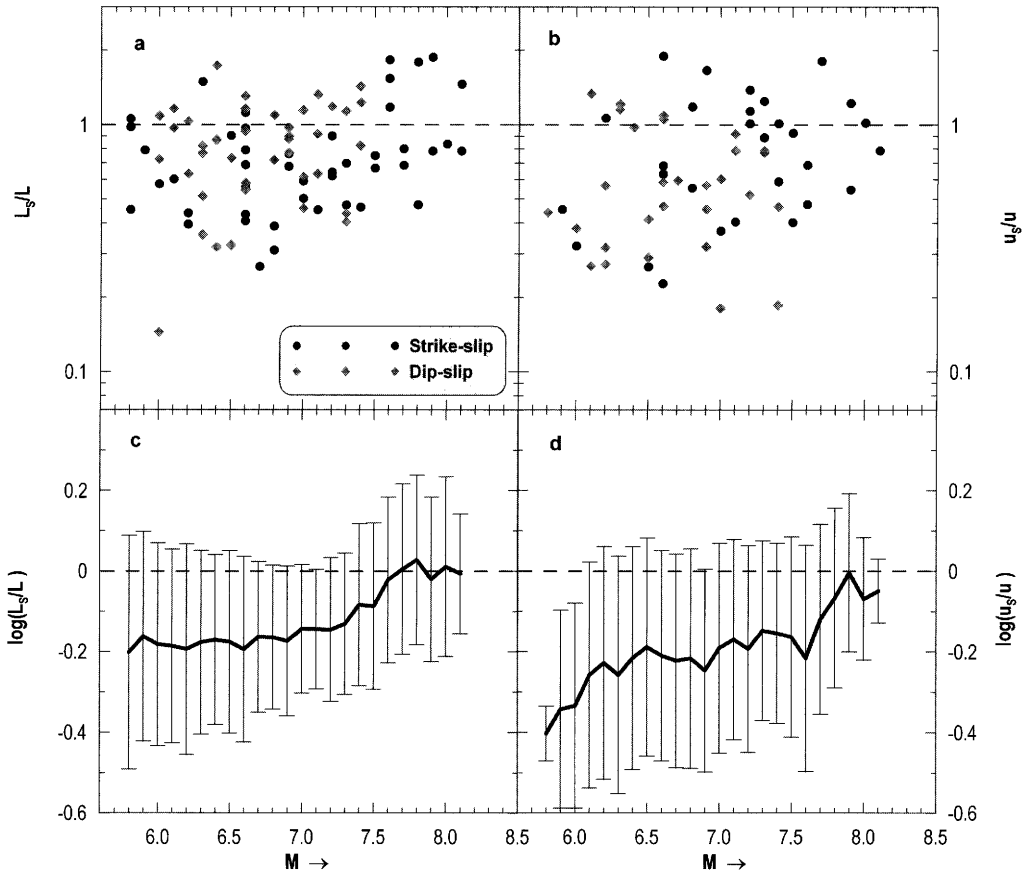

Fig. 6. Variation of the observed/true ratio of fault length (**a**) and fault-slip (**b**) v. magnitude for strike-slip and dip-slip faults. The corresponding five-point weighted moving average log-curves and their errors are shown in (**c**) and (**d**).

between strike-slip and dip-slip events, although the slip observed for dip-slip events shows somewhat smaller values than that for strike-slip events (Fig. 6b). Furthermore, a general increase of the observed/true length and slip ratios with magnitude is observed.

To further quantify this magnitude dependence, a five-point weighted moving average window of the observed ratio and its corresponding error has been estimated and is presented in Figure 6c and d. The zero-logarithm ratio line, corresponding to $L_s = L$ and $u_s = u$, is shown in both plots. In Figure 6c, the L_s/L ratio is practically constant for $5.8 \leq M \leq 7.3$, with values increasing from 66% to 71%, with an average of 69%. For larger magnitudes this L_s/L ratio increases rapidly and reaches values of *c.* 1.0 (100%) for magnitudes $M \geq 7.6$, which means that the observed fault length is practically equal to the total fault length, within statistical accuracy. On the other hand, the observed/true slip ratio exhibits a slightly different behaviour, with relatively low values for $M \leq 6.4$, increasing (more or less linearly) from *c.* 40% ($M = 5.8$) to *c.* 63% ($M = 6.4$). For magnitudes between 6.3 and 7.5 the u_s/u ratio remains practically constant at the value of *c.* 63% and then rapidly increases to almost 100% at $M \sim \geq 7.8$–7.9. Therefore, it appears that the observed/true slip ratio exhibits a similar rapid increase to almost 100% with a 'hysteresis' of *c.* 0.3 magnitude units. This 'hysteresis', together with the much larger dispersion of log (u_s/u) values compared with log (L_s/L) values and the lack of dip-slip data for $M \geq 7.5$, suggests that the use of observed slips for prediction of expected earthquake magnitude should

be performed with care and additional constraints should be used by field geologists for such estimations.

Global relations presented here allow the use of geological observations (L_s, u_s) to reliably estimate measures of earthquake size (M, L, u), necessary for earthquake prediction research. Thus, the location of active faults in the Mediterranean region, and an estimation of the seismic parameters of these faults (L, u, M) by a combined use of geological and seismological information, can be of primary importance for the application of the intermediate-term earthquake prediction method, such as that presented here. A continuous monitoring for the identification of decelerating seismic strain in each of these faults, accompanied by accelerating seismic strain in the broader region, could lead to the prediction of the origin time of the mainshock about to be generated on this fault, and its expected magnitude can be estimated by the fault dimensions.

Discussion and conclusions

Decelerating seismic strain caused by the generation of intermediate-magnitude preshocks in a seismogenic region, accompanied by accelerating seismic strain caused by the generation of larger intermediate-magnitude preshocks in the broader (critical) region, is a distinct premonitory seismicity pattern that has led to the formulation of a promising intermediate-term earthquake prediction model. This model, which can be called the 'Decelerating in–Accelerating out Seismic Strain Model', is also supported by theoretical work.

This model has been applied retrospectively to a complete set of six strong ($M \geq 6.8$) shallow mainshocks, which occurred in the Mediterranean and surrounding region (35°N–45°N, 5°W–40°E) between 1980 and 2003. All of these six mainshocks have been preceded by such patterns, which obey quantitative constraints imposed by the model. This indicates that this premonitory pattern is a general one or at least that the probability for a future large mainshock in the Mediterranean region to be preceded by such a pattern is high. This result, however, does not exclude the possibility for the occurrence of such patterns that are not followed by mainshocks (false alarms).

The model has been also applied to identify such currently occurring patterns in the Mediterranean and surrounding region, which indicate the probable generation of such strong ($M \geq 6.2$) mainshocks in this area. Nine such patterns have been observed and the estimated (predicted) parameters (origin time, epicentre coordinates, magnitude) of the corresponding, probably ensuing mainshocks are listed in Table 3. The two standard deviation model uncertainties are ± 2.5 years for the origin time, ± 0.4 for the magnitude and less than 150 km for the epicentre. There is a probability confidence of about 75% for the occurrence of each of these mainshocks, indicated by tests on synthetic catalogues (Papazachos *et al.* 2002, 2004*b*), whereas the probability for random occurrence is of the order of 10%. It should be noted that the approach used here follows that adopted in our previous studies (e.g. Papazachos & Papazachos 2000, 2001; Papazachos *et al.* 2004*a*,*b*, 2005, 2006), which is based on the critical earthquake model that is widely used in related work (e.g. Bufe & Varnes 1993; Bowman *et al.* 1998; Jaume & Sykes 1999). However, the results obtained in the present work represent our first attempt at a forward test of the proposed model, where observations during the next decade will show the degree of validity of this forward test and of the applied method.

Globally valid relations have been derived between the surface fault length, L_s, derived from geological observations and real (subsurface) fault length, L, and the mainshock magnitude, M, separately for strike-slip faults and for dip-slip faults in continental regions. Similar relations have been also derived for the surface fault slip, u_s. From the results of the prediction model previously presented, it is clear that the associated uncertainties and false-alarm rates can often lead to ambiguous results concerning the candidate neotectonic fault that will produce the expected earthquake. For this reason, it is necessary to approach the proposed method as a tool for intermediate-term time-dependent seismic hazard estimation, rather than as an accurate individual earthquake prediction method. However, the previously defined scaling relations may even help to narrow the number or spatial extent of neotectonic faults that can be associated with expected earthquakes. Thus geological observations can be used to locate active faults in the Mediterranean and through such relations to define the dimension of each such fault and the magnitude of the next oncoming mainshock in the fault. Continuous seismological monitoring of all known active faults in the Mediterranean and the identification of seismogenic regions where decelerating strain occurs (when accelerating strain occurs in the broad critical region) can lead to prediction of the next mainshock in each of these faults. The advantage of this method is that it requires data of intermediate-magnitude shocks (e.g. $M \geq 4.0$), which are easily obtained by the existing seismological networks.

Because the potential of the model examined for predicting mainshocks is still under investigation, the present work must be considered as part of the model testing. Independently, however, of the model capacity for predicting mainshocks, it is of importance for dealing with the problem of time-dependent seismic hazard assessment, as this model reliably defines critical regions, which are at a seismic excitation for a predicted time interval as a result of the generation of intermediate-magnitude shocks. The largest of these shocks (with $M \sim 6$) often cause considerable damage when their epicentres are on land (e.g. the Athens 1999 $M = 5.9$ shock killed 143 people and caused extensive destruction).

The results of the present work, which concern expected mainshocks, will be updated regularly as new observations are expected to accumulate over the next few years. Eventually, any significant change of the currently observed seismicity behaviour will be noticed and taken into consideration during the final tests.

We would like to thank Wessel & Smith (1995) for freely distributing the GMT software that was used to produce the maps of the present study. This research was partially supported by the Earthquake Protection and Planning Organization of Greece (project 20242, Res. Comm. AUTH). This paper benefited from the comments of two reviewers.

References

AMBRASEYS, N. N. & JACKSON, J. A. 1998. Faulting associated with historical and recent earthquakes in the Eastern Mediterranean region. *Geophysical Journal International*, **133**, 390–406.

ANDERSON, H. & JACKSON, J. 1987. Active tectonics of the Adriatic Region. *Geophysical Journal of the Royal Astronomical Society*, **91**, 937–983.

ANDRIEUX, J., FONBOTE, J. M. & MATTAUER, M. 1971. Sur un modè le explicatif de l'Arc de Gibraltar. *Earth and Planetary Science Letters*, **12**, 191–198.

BOWMAN, D. D., QUILLON, G., SAMMIS, C. G., SORNETTE, A. & SORNETTE, D. 1998. An observational test of the critical earthquake concept, *Journal of Geophysical Research*, **103**, 24359–24372.

BUFE, C. G. & VARNES, D. J. 1993. Predictive modeling of seismic cycle of the Great San Francisco Bay Region. *Journal of Geophysical Research*, **98**, 9871–9883.

BUFE, C. D., NISHENKO, S. P. & VARNES, D. J. 1994. Seismicity trends and potential for large earthquakes in Alaska–Aleutian region. *Pure and Applied Geophysics*, **142**, 83–99.

BUFORN, E., UDIAS, A. & MEZCUA, J. 1988*a*. Seismicity and focal mechanisms in South Spain. *Bulletin of the Seismological Society of America*, **78**, 2008–2024.

BUFORN, E., UDIAS, A. & COLOMBAS, M. A. 1988*b*. Seismicity, source mechanisms and tectonics of the Azores–Gibraltar plate boundary. *Tectonophysics*, **152**, 89–118.

DERCOURT, J., ZONENSHAIN, L. P., RICOU, L.-E., *et al.* 1986. Geological evolution of the Tethys belt from the Atlantic to the Pamirs since the Lias. *Tectonophysics*, **123**, 241–315.

DEWEY, J. F. 1988. Extensional collapse of orogens. *Tectonics*, **7**, 1123–1139.

DEWEY, J. F. & ŞENGÖR, A. M. C. 1979. Aegean and surrounding regions: complex multiplate and continuum tectonics in a convergent zone. *Geological Society of America Bulletin*, **90**, 84–92.

EVISON, F. F. 2001. Long-range synoptic earthquake forecasting: an aim for the millennium. *Tectonophysics*, **333**, 207–215.

FACCENNA, C., DAVY, P., BRUN, J. P., FUNICIELLO, R., GIARDINI, D., MATTEI, M. & NALPAS, T. 1996. The dynamics of back-arc extension: an experimental approach to the opening of the Tyrrhenian Sea. *Geophysical Journal International*, **126**, 781–795.

FACCENNA, C., BECKER, T. W., LUCENTE, F. P., JOLIVET, L. & ROSSETTI, F. 2001. History of subduction and back-arc extension in the Central Mediterranean. *Geophysical Journal International*, **145**, 809–820.

FUJII, Y. & MATSUURA, M. 2000. Regional difference in scaling laws for large earthquakes and its tectonic implication. *Pure and Applied Geophysics*, **157**, 2283–2302.

GASPARINI, G., IANNACCONE, G. & SCARPA, R. 1985. Fault-plane solutions and seismicity of the Italian peninsula. *Tectonophysics*, **117**, 59–78.

HAINZL, S., ZOLLER, G., KURTHS, J. & ZSCHAU, J. 2000. Seismic quiescence as an indicator for large earthquakes in a system of self-organized criticality. *Geophysical Research Letters*, **27**, 597–600.

HENRY, C. & DAS, S. 2001. Aftershock zones of large shallow earthquakes: fault dimensions, aftershock area expansion and scaling relation. *Geophysical Journal International*, **147**, 272–293.

JACKSON, J. & MCKENZIE, D. 1988. The relationship between plate motions and seismic moment tensors and the rates of active deformation in the Mediterranean and Middle East. *Geophysical Journal of the Royal Astronomical Society*, **93**, 45–73.

JAUMÉ, S. C. & SYKES, L. R. 1999. Evolving towards a critical point: a review of accelerating seismic moment/energy release rate prior to large and great earthquakes. *Pure and Applied Geophysics*, **153**, 279–306.

JIMENEZ-MUNT, I. & NEGREDO, A. 2003. Neotectonic modeling of the western part of the Africa–Eurasia plate boundary: from the mid-Atlantic ridge to Algeria. *Earth and Planetary Science Letters*, **205**, 257–271.

JOLIVET, L. & FACCENNA, C. 2000. Mediterranean extension and the Africa–Eurasia collision. *Tectonics*, **19**, 1095–1107.

KAHLE, H.-G., STRAUB,C., REILINGER, R., *et al.* 1998. The strain field in the eastern Mediterranean estimated by repeated GPS measurements. *Tectonophysics*, **294**, 237–252.

KATO, N., OTHAKE, M. & HIRASAWA, T. 1997. Possible mechanism of precursory seismic quiescence: regional stress relaxation due to preseismic sliding. *Pure and Applied Geophysics*, **150**, 249–267.

KNOPOFF, L., LEVSHINA, T., KEYLLIS-BOROK, V. J. & MATTONI, C. 1996. Increased long-range intermediate-magnitude earthquake activity prior to strong earthquakes in California. *Journal of Geophysical Research*, **101**, 5779–5796.

LEPICHON, X. & ANGELIER, J. 1979. The Hellenic arc and trench system: a key to the neotectonic evolution of the eastern Mediterranean area. *Tectonophysics*, **60**, 1–42.

MALINVERNO, A. & RYAN, W. B. F. 1986. Extension in the Tyrrhenian Sea and shortening in the Apennines as result of arc migration driven by sinking of the lithosphere. *Tectonics*, **5**, 227–245.

MCCLUSKY, S., BALASSANIAN, S., BARKA, A., *et al.* 2000. Global Positioning System constraints on plate kinematics and dynamics in the eastern Mediterranean and Caucasus. *Journal of Geophysical Research*, **105**, 5695–5719.

MCKENZIE, D. P. 1970. The plate tectonics of the Mediterranean region. *Nature*, **226**, 239–243.

MCKENZIE, D. P. 1972. Active tectonics of the Mediterranean region. *Geophysical Journal of The Royal Astronomical Society*, **30**, 109–185.

MEIJER, P. T. & WORTEL, M. J. R. 1997. Present-day dynamics of the Aegean region: a model analysis of the horizontal pattern of stress and deformation. *Tectonics*, **16**, 879–895.

MERCIER, J. L., CAREY, E., PHILIP, H. R. & SOREL, D. 1976. La néotectonique plio-quaternaire de l'arc egéen externe et de la Mer egéen et ses relations avec seismicité. *Bulletin de la Société Géologique de France*, **18**, 159–176.

MERCIER, J. L., SOREL, D., VERGÉLY, P. & SIMEAKIS, K. 1989. Extentional tectonic regimes in the Aegean basins during the Cenozoic. *Basin Research*, **2**, 49–71.

MOGI, K. 1969. Some features of the recent seismic activity in and near Japan II. Activity before and after great earthquakes. *Bulletin of Earthquake Research Institute, University of Tokyo*, **47**, 395–417.

PAPADOPOULOS, G. A. 1986. Long term earthquake prediction in western Hellenic arc. *Earthquake Prediction Research*, **4**, 131–137.

PAPAZACHOS, B. C. 1990. Seismicity of the Aegean and surrounding area. *Tectonophysics*, **178**, 287–308.

PAPAZACHOS, B. C. & PAPAZACHOS, C. B. 2000. Accelerated preshock deformation of broad regions in the Aegean area. *Pure and Applied Geophysics*, **157**, 1663–1681.

PAPAZACHOS, B. C. & PAPAZACHOU, C. B. 2003. *The Earthquakes of Greece*. Ziti, Thessaloniki.

PAPAZACHOS, B. C., PAPADIMITRIOU, E. E., KIRATZI, A. A., PAPAZACHOS, C. B. & LOUVARI, E. K. 1998. Fault plane solutions in the Aegean Sea and the surrounding area and their tectonic implications. *Bollettino di Geofisica Teorica ed Applicata*, **39**, 199–218.

PAPAZACHOS, B. C., SCORDILIS, E. M., PANAGIOTOPOULOS, D. G., PAPAZACHOS, C. B. & KARAKAISIS, G. F. 2004*c*. Global relations between seismic fault parameters and moment magnitude of earthquakes. *Bulletin of the Geological Society of Greece*, **25**, 1–8.

PAPAZACHOS, B. C., COMNINAKIS, P. E., SCORDILIS, E. M., KARAKAISIS, G. F. & PAPAZACHOS, C. B. 2005. *A catalogue of earthquakes in the Mediterranean and surrounding area for the period 1901–2004.* Publication Geophysical Laboratory, University of Thessaloniki. http://lemnos.geo.auth.gr/the_seisnet/medcatalog.txt

PAPAZACHOS, C. B. & KIRATZI, A. A. 1996. A detailed study of the active crustal deformation in the Aegean and surrounding area. *Tectonophysics*, **253**, 129–153.

PAPAZACHOS, C. B. & PAPAZACHOS, B. C. 2001. Precursory accelerating Benioff strain in the Aegean area. *Annali di Geofisica*, **144**, 461–474.

PAPAZACHOS, C. B., KARAKAISIS, G. F., SAVVAIDIS, A. S. & PAPAZACHOS, B. C. 2002. Accelerating seismic crustal deformation in the southern Aegean area. *Bulletin of the Seismological Society of America*, **92**, 570–580.

PAPAZACHOS, C. B., KARAKAISIS, G. F., SCORDILIS, E. M. & PAPAZACHOS, B. C. 2004*a*. Probabilities of activation of seismic faults in critical regions of the Aegean area. *Geophysical Journal International*, **159**, 679–687.

PAPAZACHOS, C. B., SCORDILIS, E. M. KARAKAISIS, G. F. and PAPAZACHOS, B. C. 2004*b*. Decelerating preshock seismic deformation in fault regions during critical periods, *Bulletin of the Geological Society of Greece*, **36**, 1–9.

PAPAZACHOS, C. B., KARAKAISIS, G. F., SCORDILIS, E. M. & PAPAZACHOS, B. C. 2005. Global observational properties of the critical earthquake model. *Bulletin of the Seismological Society of America*, **95**, 1841–1855.

PAPAZACHOS, C. B., KARAKAISIS, G. F., SCORDILIS, E. M. & PAPAZACHOS, B. C. 2006. New observational information on the precursory accelerating and decelerating strain energy release. *Tectonophysics*, doi: 10.1016/j.tecto.2006.03.004.

PAVLIDES, S. & CAPUTO, R. 2004. Magnitudes versus faults' surface parameters: quantitative relationships from the Aegean region. *Tectonophysics*, **380**, 159–188.

PEGLER, G. & DAS, S. 1996. Analysis of the relationship between seismic moment and fault length for large crustal strike-slip earthquakes between 1977–92. *Geophysical Research Letters*, **23**, 905–908.

SCORDILIS, E. M. 2006. Empirical global relations for MS, mb, ML, and moment magnitude. *Journal of Seismology*, doi: 10.1007/S10950-006-9012-4.

SORNETTE, A. & SORNETTE, D. 1990. Earthquake rupture as a critical point. Consequences for telluric precursors. *Tectonophysics*, **179**, 327–334.

SORNETTE, D. & SAMMIS, C. G. 1995. Complex critical exponents from renormalization group theory of earthquakes: implications for earthquake predictions. *Journal of Physics Series I.*, **5**, 607–619.

STOCK, C. & SMITH, E. G. V. 2000. Evidence for different scaling of earthquake source parameters for

large earthquakes depending on fault mechanism. *Geophysical Journal International*, **143**, 157–162.

SYKES, L. R. & JAUMÉ, S. 1990. Seismic activity on neighboring faults as a long term precursor to large earthquakes in the San Francisco Bay area. *Nature*, **348**, 595–599.

TAYMAZ, T., JACKSON, J. & MCKENZIE, D. 1991. Active tectonics of the north and central Aegean Sea. *Geophysical Journal International*, **106**, 433–490.

TOCHER, D. 1959. *Seismic history of the San Francisco bay region*. California Division of Mines Special Report, **57**, 39–48.

TZANIS, A., VALLIANATOS, F. & MAKROPOULOS, K. 2000. Seismic and electrical precursors to the 17-1-1983, M = 7 Kefallinia earthquake, Greece, signatures of a SOC system. *Physics and Chemistry of the Earth*, **25**, 281–287.

WELLS, D. L. & COPPERSMITH, K. J. 1994. New empirical relationships among magnitude, rupture length, rupture width, rupture area and surface displacement. *Bulletin of the Seismological Society of America*, **84**, 974–1002.

WESSEL, P. & SMITH, W. 1995. New version of the Generic Mapping Tools. *EOS Transactions, American Geophysical Union*, **76**, 329.

WORTMANN, U. G., WEISSERT, H., FUNK, H. & HAUCK, J. 2001. Alpine plate kinematics revisited: the Adrian problem. *Tectonics*, **20**, 134–147.

WYSS, M. 1997. Cannot earthquakes be predicted? *Science*, **278**, 487–488.

WYSS, M. & HABERMANN, R. E. 1988. Precursory seismic quiescence. *Pure and Applied Geophysics*, **126**, 319–332.

WYSS, M., KLEIN, F. & JOHNSTON, A. C. 1981. Precursors of the Kalapana M = 7.2 earthquake. *Journal of Geophysical Research*, **86**, 3881–3900.

ZÖLLER, G., HAINZL, S., KURTHS, J. & ZSCHAU, J. 2002. A systematic test on precursory seismic quiescence in Armenia. *Natural Hazards*, **26**, 245–263.